Reproductive and Developmental Medicine®

Atp6v0d2 deficiency partially restores defects in *Mcoln1*-deficient mouse corpus luteum

Yuehuan Li[1], Ahmed E. El Zowalaty[1,2], Jonathan Matthew Hancock[1,2], Zidao Wang[1,2], Taylor Elijah Martin[1,2], Tingjie Zhan[3], Yingzheng Wang[3], Christian Lee Andersen[1,2], Suvitha Viswanathan[1], Jaymie Bromfield[1], Venkata Abhigna Atluri[1], Karly Rae Kallish[1], Hope Nicole Grismer[1], Shuo Xiao[3], Xiaoqin Ye[1,2,*]

Abstract

Objective: ATP6V0d2 is a subunit of the vacuolar-type H^+-ATPase (V-ATPase) that pumps H^+ ions into lysosomes. TRPML1 (*MCOLN1/Mcoln1*) transports cations out of lysosomes. *Mcoln1*$^{-/-}$ mice recapitulate the lysosomal storage disorder mucolipidosis type IV (MLIV) phenotype. We previously demonstrated that *Mcoln1*$^{-/-}$ female mice quickly became infertile at 5 months old (5M) with degenerating corpora lutea (CL) and progesterone (P4) deficiency. We tested our hypothesis that *Atp6v0d2* deficiency could partially compensate for *Mcoln1* deficiency to restore CL functions in *Atp6v0d2*$^{-/-}$*Mcoln1*$^{-/-}$ mice.

Methods: Control and *Atp6v0d2*$^{-/-}$*Mcoln1*$^{-/-}$ female mice underwent fertility test from 2M to 7M. A subset of them was dissected at 5M on day 3.5 post-coitum (D3.5). The D3.5 ovaries from 5M control, *Mcoln1*$^{-/-}$, and *Atp6v0d2*$^{-/-}$*Mcoln1*$^{-/-}$ mice were evaluated for CL morphology, lipid droplet staining, and markers of mitochondria and P4 steroidogenesis in the luteal cells.

Results: The fertility test of *Atp6v0d2*$^{-/-}$*Mcoln1*$^{-/-}$ female mice (2M–7M) revealed normal mating activity but reduced fertility compared with the control; yet ~25% of them remained fertile at 5M to 7M but with dystocia. We analyzed a subset of 11 *Atp6v0d2*$^{-/-}$*Mcoln1*$^{-/-}$ mice (5M) in the fertility test on D3.5: three (27.3%) had normal P4 levels and all examined CL parameters, indicating full restoration of CL function compared with *Mcoln1*$^{-/-}$, whereas eight had P4 deficiency, with two (18.2%) infertile and six (54.5%) once fertile. In contrast to *Mcoln1*$^{-/-}$ CLs, which had extensive amorphous cellular debris, indicating cell degeneration, *Atp6v0d2*$^{-/-}$*Mcoln1*$^{-/-}$ CLs had reduced amorphous cellular debris regardless of P4 levels. However, similar to *Mcoln1*$^{-/-}$ CLs, P4-deficient *Atp6v0d2*$^{-/-}$*Mcoln1*$^{-/-}$ CLs showed impaired differentiation, enlarged lipid droplets, disorganized expression of endothelial basal lamina marker collagen IV, and reduced expression of mitochondrial marker heat shock protein 60 (HSP60) and steroidogenesis rate-limiting protein StAR, indicating that additional *Atp6v0d2* deficiency compensates for *Mcoln1* deficiency-induced cell degeneration, but is insufficient to restore luteal cell differentiation and P4 steroidogenesis in P4-deficient *Atp6v0d2*$^{-/-}$*Mcoln1*$^{-/-}$ CLs.

Conclusion: This study shows that *Atp6v0d2*$^{-/-}$*Mcoln1*$^{-/-}$ CLs had varied improvements compared with *Mcoln1*$^{-/-}$ CLs, and it provides *in vivo* genetic evidence of the coordination between different lysosomal channels in CL function.

Keywords: ATP6V0D2/*Atp6v0d2*, TRPML1/*Mcoln1*, *Atp6v0d2*$^{-/-}$*Mcoln1*$^{-/-}$ mice, Progesterone, Corpus luteum

Introduction

Lysosomes are acidic, membrane-bound intracellular organelles[1–3]. The lysosomal lumen has a pH of ~4.6, and the intracellular pH is generally ~7.0 to 7.4. Lysosomal acidity is critical for lysosomal enzymes to degrade macromolecules and maintain normal cellular homeostasis. The lysosomal lumen has higher [H^+], [Ca^{2+}], [Na^+], and [Cl^-], but lower [K^+] than the cytosol. Approximately 500-fold [H^+] gradient across the lysosomal membrane is established and maintained by the vacuolar-type H^+-ATPase (V-ATPase), which pumps H^+ into the lysosomal lumen[1–3]. Lysosomal counter ion channels and transporters dissipate the transmembrane voltage generated by V-ATPase to maintain lysosomal ionic homeostasis and membrane potential[4]. These include the transient receptor potential cation channels of the mucolipin subfamily 1–3 (TRPML1–3, the primary lysosomal Ca^{2+} release channels), Na^+-selective two-pore channels 1 and 2 (TPC1–2), and various channels/transporters for conducting Cl^-, K^+, and catabolites, etc.[4]. Lysosomes have essential functions in digestion, signaling, trafficking, etc., and disrupted lysosomal functions are associated with >50 rare inherited metabolic disorders in humans, collectively termed lysosomal storage diseases[1–5].

Our research on early pregnancy, such as uterine receptivity for embryo implantation[6,7], led us to investigate the lysosome, including lysosomal function in the corpus luteum (CL) for progesterone (P4) synthesis to support early pregnancy[8–12]. Embryo implantation is initiated when a competent embryo attaches

[1]Department of Physiology and Pharmacology, College of Veterinary Medicine, University of Georgia, Athens, GA 30602, USA; [2]Interdisciplinary Toxicology Program, University of Georgia, Athens, GA 30602, USA; [3]Department of Pharmacology and Toxicology, Ernest Mario School of Pharmacy, Environmental and Occupational Health Sciences Institute (EOHSI), Rutgers University, Piscataway, NJ 08854, USA.

*Corresponding to: Xiaoqin Ye, Department of Physiology and Pharmacology, College of Veterinary Medicine; Interdisciplinary Toxicology Program, University of Georgia, 501 DW Brooks Dr., Athens, GA 30602, USA. E-mail: ye@uga.edu

Reproductive and Developmental Medicine (2025) 9:1

Received: 4 September 2024 **Accepted:** 5 December 2024

http://dx.doi.org/10.1097/RD9.0000000000000116

to the uterine luminal epithelium (LE), which occurs approximately 4 days post-coitum (D4.0) in mice. Microarray analysis (GEO number: GSE44451) of D3.5 and D4.5 mouse uterine LE revealed *Atp6v0d2*, a previously uncharacterized gene in the LE, to be one of the most upregulated genes on embryo implantation initiation[9]. *Atp6v0d2* is also among the earliest response genes in the uterus sensing the presence of embryos approaching embryo attachment (GEO number: GSE247638)[13]. The differential expression of *Atp6v0d2* led to the novel finding of uterine epithelial acidification, which is detected using LysoSensor Green DND-189, on embryo implantation initiation in mice[10]. Mice deficient of *Atp6v0d2* (*Atp6v0d2*$^{-/-}$) exhibit impaired osteoclast fusion and increased bone formation[14]. *Atp6v0d2*$^{-/-}$ female mice have a significantly reduced embryo implantation rate and marginally reduced delivery rate from the first mating only (2 months old, 2M), and have normal fertility thereafter[10]. The ability of V-ATPase inhibitor bafilomycin on disrupting uterine receptivity, coupled with LE acidification on initiation of embryo implantation, has established the important role of V-ATPase in uterine receptivity for embryo implantation[10].

V-ATPase has a transmembrane integral V0 domain for proton (H^+) translocation and a cytoplasmic peripheral V1 domain for ATP hydrolysis[15,16]. The V0 domain includes subunits a, c, c″, d, e, which are encoded by *ATP6V0* genes, and accessory subunits Ac45 (*ATP6VAP1*) and M8–9 (*ATP6VAP2*)[17]. The V1 domain contains subunits A–H, which are encoded by *ATP6V1* genes. The d subunit of the V0 domain connects the V0 and V1 domains and forms a rotor with the D and F subunits of the V1 domain. Rotor rotation is powered by ATP hydrolysis[15]. The d subunit is encoded by two genes: the more ubiquitously expressed *Atp6v0d1* and the more tissue-specific *Atp6v0d2*[16]. V-ATPase pumps H^+ from the cytoplasmic compartment to the opposite side of the membrane where it is localized, which can be the plasma membrane or the membranes of intracellular organelles, to acidify the extracellular environment or the lumen of the intracellular organelles, respectively[18].

The function of V-ATPase in acidifying the lysosomal lumen requires counterion channels. Before the recent finding that LRRC8 family proteins (components of volume-regulated anion channels [VRACs]), which have known functions in the plasma membrane, also act within lysosomes[19], our microarray analysis showed that *Mcoln1* had the highest mRNA expression level in the peri-implantation LE (GEO number: GSE44451[9]) among the known and putative lysosomal counter ion channels/transporters that were summarized recently[2]. *MCOLN1*/*Mcoln1* encodes TRPML1 (transient receptor potential cation channel, mucolipin subfamily, member 1), which is an important lysosomal counter cation channel, and its critical lysosomal functions have been established in both humans and mice[4,20–23]. Although an earlier report indicated that *Mcoln1*$^{-/-}$ female mice were fertile[23], our systemic fertility study demonstrated that *Mcoln1*$^{-/-}$ female mice had normal mating activities but reduced fertility at 2M, and quickly became infertile at 5M with P4 deficiency, which was caused by defective CL integrity and function[11].

TRPML1 mediates the release of cations (e.g., Ca^{2+}, Na^+, and Fe^{2+}) from the lysosomal lumen to the cytosol to dissipate the transmembrane voltage built up by V-ATPase, thus indirectly regulating lysosomal lumen acidity[4,5,24]; or it permits H^+ to leak out of the lysosome, thus directly regulating the lysosomal lumen acidity[25]. TRPML1 is also critical for vesicular trafficking, lipid homeostasis, autophagy, plasma membrane repair, and signaling during cellular adaptation to nutrient availability, etc.[5,24]. TRPML1 deficiency leads to mucolipidosis type IV (MLIV) in both humans and mice[4,20–23]. *Mcoln1*$^{-/-}$ mice recapitulate phenotypes associated with MLIV, such as neurodegeneration, ophthalmologic abnormalities, and muscular dystrophy[21,23].

Lysosomal functions, such as H^+ pumping by V-ATPase, require the maintenance of lysosomal lumen ionic homeostasis and membrane potential[4]. Acidification of the lysosomal lumen by V-ATPase is important for the function of most lysosomal hydrolases and requires a balanced efflux of countercations and/or influx of counteranions to compensate for the influx of H^+ by V-ATPase. Because TRPML1 is an important counter ion channel to efflux cations from the lysosome, and ATP6V0d2 is 1 of the 2 V0 d subunits for V-ATPase, we hypothesized that additional deletion of *Atp6v0d2* in *Mcoln1*$^{-/-}$ female mice would partially cancel out the overly acidic lysosomal lumen caused by *Mcoln1* deficiency[25] thus alleviating the defects in *Mcoln1*$^{-/-}$ CLs[11]. We tested this hypothesis in *Atp6v0d2*$^{-/-}$*Mcoln1*$^{-/-}$ double-knockout mice.

Materials and methods

Animals and genotyping

Atp6v0d2$^{-/-}$*Mcoln1*$^{-/-}$ mice were produced by breeding *Atp6v0d2*$^{+/-}$ mice[10], which were derived from Dr. Yongwon Choi's colony at the University of Pennsylvania[14], with *Mcoln1*$^{+/-}$ mice[11], which were purchased from The Jackson Laboratory (B6.Cg-Mcoln1tm1Sasl/J Stock No: 027110, Bar Harbor, ME, USA[23]). Mice with the genotypes *Atp6v0d2*$^{+/+}$*Mcoln1*$^{+/+}$ (wild-type), *Atp6v0d2*$^{+/-}$*Mcoln1*$^{+/+}$, *Atp6v0d2*$^{+/+}$*Mcoln1*$^{+/-}$, and *Atp6v0d2*$^{+/-}$*Mcoln1*$^{+/-}$ have normal fertility and were used as controls. Polymerase chain reaction was used for genotyping as previously described[10,11]. All mice were housed in polypropylene cages on a 12-hour light/dark cycle (6:00–18:00) at 23 ± 1°C with 30% to 50% relative humidity. All mice had free access to regular food and water. The study protocol was approved by the University of Georgia Institutional Animal Care and Use Committee (IACUC) and conformed to the National Institutes of Health guidelines and federal law.

Mating and fertility tests

Mcoln1$^{-/-}$ female mice quickly become infertile at 5M[11]. For comparison, *Atp6v0d2*$^{-/-}$*Mcoln1*$^{-/-}$ female mice were tracked for mating and fertility from 2M to up to 7M. The reduction of mice in the cohort toward the end of tracking was mainly because of random selection for serum collection at 5M and sacrificing at various ages following the COVID-19 lockdown policy. Control female mice ($n = 29$) and *Atp6v0d2*$^{-/-}$*Mcoln1*$^{-/-}$ female mice ($n = 40$) aged 2M cohabited with the same wild-type stud males. Each stud male was housed with two *Atp6v0d2*$^{-/-}$*Mcoln1*$^{-/-}$ females and two control females. Each female was checked every morning for the presence of a vaginal plug that indicates mating during the previous night. The day of vaginal plug detection was designated as day 0.5 post-coitum (D0.5, the mating night as D0). The females with a vaginal plug were weighed every 3 days from D0.5 to D18.5. They continued cohabitation with their respective stud males and were checked for a vaginal plug every morning until a steady weight gain was observed to confirm pregnancy. Each confirmed pregnant female was then housed separately, and its body weight was monitored until delivery. Some females were plugged multiple times before a pregnancy could be confirmed by the body weight gain; some pregnant females would stop gaining weight and end up losing

the pregnancy; and some females were plugged multiple times but never showed body weight gain associated with pregnancy, and they were infertile. The plugging rate (the percentage of mice in each group with the presence of a vaginal plug), plugging latency (the duration from cohabitation to the detection of the first vaginal plug), post-mating body weight gain, gestational period (the duration from mating to delivery), litter size, and pregnancy rate were recorded. Pregnancy age was defined as the age at which mating occurred. For example, if a pregnancy was derived from a mating (indicated by the presence of a vaginal plug) before 3M, the pregnancy age was 2M; likewise, the pregnancy age of 5M was from mating after 5M but before 6M; and the pregnancy age of 6 to 7M was from mating after 6M but before 8M. The pregnancy rate was calculated as the percentage of mated females in the same mating age group (2M, 5M, or 6–7M) that had a confirmed pregnancy, as indicated by a steadily increasing body weight 6 days post-coitum.

Serum P4 and E_2 measurement

At 5M, day 3.5 post-coitum (D3.5) control mice ($n = 4$) and *Atp6v0d2*$^{-/-}$*Mcoln1*$^{-/-}$ mice ($n = 11$) in the fertility test were randomly selected, with the latter including nine mice that had delivered at least one litter and two mice that had mating activities indicated by multiple vaginal plugs but had never delivered pups or showed body weight gain associated with pregnancy. Between 11:00 and 12:00 hours, D3.5 mice were anesthetized *via* isoflurane inhalation for blood collection *via* the orbital sinus. Serum was collected after blood clotting at room temperature for 45 minutes and stored at –80°C. One ovary was fixed in 10% formalin solution, and the other was snap-frozen. Serum P4 and 17β-E_2 levels were measured using the Ligand Assay and Analysis Core of the Center for Research in Reproduction at the University of Virginia (Charlottesville, VA, USA).

Ovary histology

The fixed ovaries were maintained in a fixative for 24 hours and then transferred to 70% ethanol. They were processed for paraffin embedding as previously described[11,26–28]. Paraffin sections (5 µm) through the widest middle portion of the ovaries were collected, processed, and stained with hematoxylin and eosin. Follicles at different stages, the number of CLs in each section, and the morphology of each CL (e.g., luteal cord, amorphous cell debris, luteal cell cytoplasm, and luteal cell vacuolization, etc.) were analyzed as described previously[11,26,29].

Immunofluorescence

Immunofluorescence was used to detect collagen IV (Col IV), heat shock protein 60 (HSP60), and steroidogenic acute regulatory protein (StAR) in 5M D3.5 control, *Mcoln1*$^{-/-}$, and *Atp6v0d2*$^{-/-}$*Mcoln1*$^{-/-}$ frozen ovarian sections (10 µm) as previously described[26]. Briefly, frozen sections were fixed in 4% paraformaldehyde and subjected to antigen retrieval in 0.01M sodium citrate (pH 6.0) at 95°C for 20 minutes. The sections were washed with 1× phosphate-buffered saline (1× PBS) followed by membrane permeabilization with 0.15% Triton X-100. The slides were then washed and blocked with 10% goat serum for 1 hour at room temperature and incubated with anti-Col IV (5 µg/mL, Abcam, ab19808, Cambridge, UK), anti-HSP60 (1:500, Cell Signaling Technology, mAb #12165, Danvers, MA, USA), or anti-StAR (1:500, Abcam, ab96637, Cambridge, UK) overnight at 4°C. On the following day, the sections were washed in 1× PBS and incubated with secondary Alexa Fluor-conjugated goat anti-rabbit immunoglobulin G (10 µg/mL, Invitrogen, Waltham, MA, USA; A11036 for Col IV, A11034 for StAR, and HSP60) for 1 hour. Sections were counterstained and mounted in 4′,6′-diamino-2-phenylindole (DAPI)-containing Vectashield (Vector Laboratories, Burlingame, CA, USA).

Lipid droplet staining

Frozen ovarian sections (10 µm) were fixed in 4% paraformaldehyde at room temperature for 20 minutes, washed twice in 1× PBS, and then covered with 1.6 µg/mL Nile red (N3013, Sigma-Aldrich) in 1× PBS at room temperature for 15 minutes. Sections were then washed in 1× PBS and counterstained with DAPI[11,12,26].

Statistical analysis

Data are presented as means ± standard deviations where applicable. The Wilcoxon rank-sum test was used to assess plugging latency. For parameters with percentages, a two-tailed Fisher's exact test was used. Two-tailed unequal variance Student's *t* test and/or two-way analysis of variance (ANOVA) were conducted for other quantitative data. Significance was set at $P < 0.05$.

Results

Mating, fertility, and dystocia in *Atp6v0d2*$^{-/-}$*Mcoln1*$^{-/-}$ females

We produced *Atp6v0d2*$^{-/-}$*Mcoln1*$^{-/-}$ double-knockout mice from *Atp6v0d2*$^{+/-}$[10] and *Mcoln1*$^{+/-}$ mice[11]. In the female fertility study, virgin control female mice ($n = 29$) and *Atp6v0d2*$^{-/-}$*Mcoln1*$^{-/-}$ female mice ($n = 40$) at 2M were cohabitated with the same wild-type stud males and were checked for a vaginal plug every morning. They were all plugged within 17 days of cohabitation. The overall first plugging latencies were comparable between the control group and the *Atp6v0d2*$^{-/-}$*Mcoln1*$^{-/-}$ group (Fig. 1A). *Atp6v0d2*$^{-/-}$*Mcoln1*$^{-/-}$ mice had reduced pregnancy rates in all the three age groups compared with age-matched control groups, and the pregnancy rates at 5M and 6M to 7M were lower than that at 2M in *Atp6v0d2*$^{-/-}$*Mcoln1*$^{-/-}$ mice, but not in control mice (Fig. 1B), indicating premature reduction of fertility in *Atp6v0d2*$^{-/-}$*Mcoln1*$^{-/-}$ mice. Most pregnancies at 2M were from the first mating (23/29 in the control group and 22/29 in *Atp6v0d2*$^{-/-}$*Mcoln1*$^{-/-}$ group), and the remaining pregnancies at 2M were detected after multiple matings. The 11 *Atp6v0d2*$^{-/-}$*Mcoln1*$^{-/-}$ mice that did not yield a pregnancy at 2M after >3 vaginal plugs continued mating activities throughout the fertility test, and three of them eventually produced a litter ($n = 2$) or two litters ($n = 1$). Therefore, 8 of 40 (20%) *Atp6v0d2*$^{-/-}$*Mcoln1*$^{-/-}$ mice were born infertile, and this infertility rate was significantly higher than that of control mice (0/29 = 0%, $P = 0.0172$, two-tailed Fisher's exact test), but comparable to that of *Mcoln1*$^{-/-}$ mice (7/29 = 24%, $P = 0.7709$, two-tailed Fisher's exact test)[11].

The gestation periods were comparable between the two groups at all three time points, although those with dystocia required ≥2 days to finish delivery or were euthanized by the third day of delivery. The litter sizes were smaller in *Atp6v0d2*$^{-/-}$*Mcoln1*$^{-/-}$ mice in the 2M and 5M groups than in the age-matched control groups (6.5 ± 1.9 *vs.* 8.0 ± 2.9 at 2M, $P < 0.05$; 5.6 ± 1.9 *vs.* 8.3 ± 2.5 at 5M, $P < 0.05$). In the 6M to

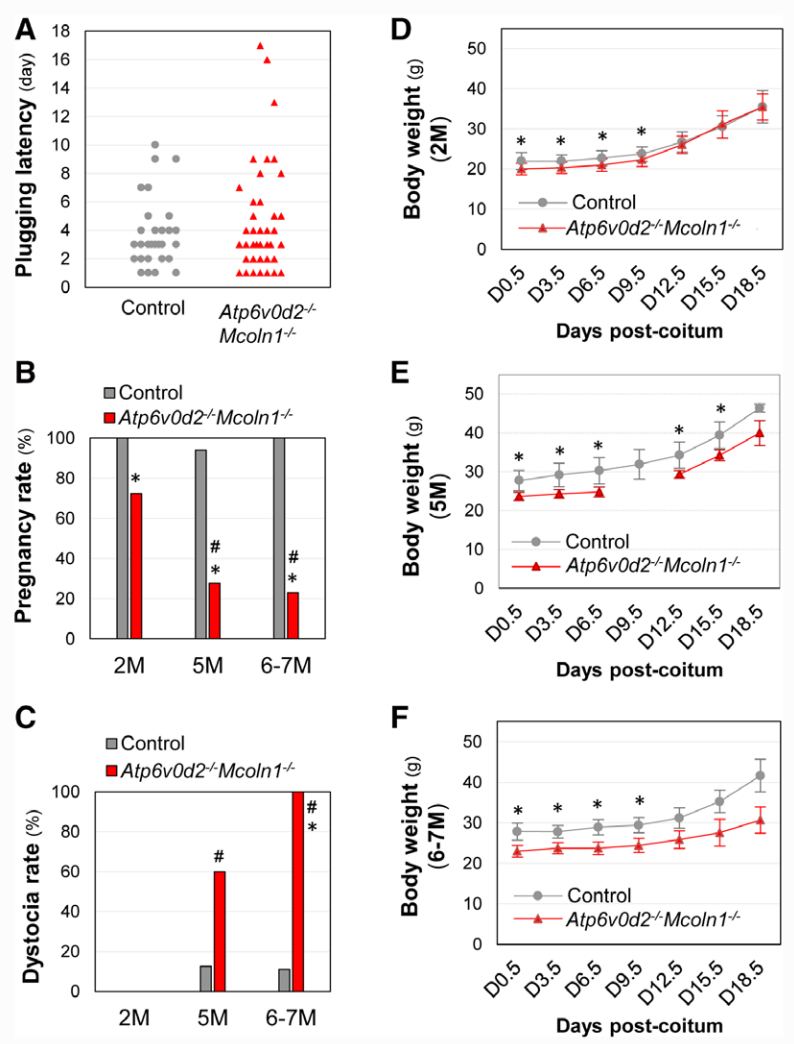

Fig. 1. Fertility test in *Atp6v0d2*$^{-/-}$*Mcoln1*$^{-/-}$ female mice. (A) Plugging latency from cohabitation to detection of the first vaginal plug. Control: gray dots, $n = 29$; *Atp6v0d2*$^{-/-}$*Mcoln1*$^{-/-}$: red triangle, $n = 40$. (B) Pregnancy rates at 2M, 5M, and 6M–7M. Pregnancy age was based on the time when a vaginal plug was detected. *P <0.05, compared with the respective control group; #P <0.05, compared with the 2M *Atp6v0d2*$^{-/-}$*Mcoln1*$^{-/-}$ group. Control: n = 29/29 (2M), 16/17 (5M), and 9/9 (6M–7M); *Atp6v0d2*$^{-/-}$*Mcoln1*$^{-/-}$: n = 29/40 (2M), 5/18 (5M), and 3/13 (6M–7M). The reduction of 12 mice in the control cohort from 2M to 5M was attributable to previous pregnancy and nursing (three mice) therefore not in mating; sickness therefore euthanized (one mouse); dissection for D3.5 serum collection at 5M (four mice); and being sacrificed following COVID-19 lockdown policy (four mice). The reduction of eight mice in the control cohort from 5M to 6–7M was because of previous pregnancy and nursing (one mouse) therefore not in mating; and being sacrificed following COVID-19 lockdown policy (seven mice). The reduction of 22 mice in the *Atp6v0d2*$^{-/-}$*Mcoln1*$^{-/-}$ cohort from 2M to 5M was because of previous pregnancy and nursing (one mouse) therefore not in mating; death (one mouse); dissection for D3.5 serum collection at 5M (11 mice); and being sacrificed following COVID-19 lockdown policy (nine mice). The reduction of five mice in the *Atp6v0d2*$^{-/-}$*Mcoln1*$^{-/-}$ cohort from 5M to 6M–7M was because of death before 6M (two mice); and being sacrificed following COVID-19 lockdown policy (three mice). (C) Dystocia rates at 2M, 5M, and 6M–7M. *P <0.05, compared with the respective control group; #P <0.05, compared with the 2M *Atp6v0d2*$^{-/-}$*Mcoln1*$^{-/-}$ group. (D–F) Body weight change during pregnancy at pregnancy ages of 2M (D), 5M (E), and 6M–7M (F). The numbers of pregnant mice with body weight data were 22, 11, and 5 for the control groups and 26, 4, and 3 for the *Atp6v0d2*$^{-/-}$*Mcoln1*$^{-/-}$ groups, respectively. One missing data point in (E) was because of incomplete collection of the body weight data. Error bar, standard deviation; *P <0.05, compared with the respective control group at the same post-coitum day, two-tailed unequal variance student t test; or $P = 0.001$ (2M, D), P <0.001 (5M, E), and P <0.001 (6M–7M, F), two-way analysis of variance.

7M group, all pups from pregnant *Atp6v0d2*$^{-/-}$*Mcoln1*$^{-/-}$ mice were stillbirths because of dystocia (Fig. 1C). Dystocia was observed in approximately 10% of term pregnant control mice in the 5M and 6M to 7M groups, as well as in 60% (3/5, 5M) and 100% (3/3, 6–7M) of term pregnant *Atp6v0d2*$^{-/-}$*Mcoln1*$^{-/-}$ mice (Fig. 1C).

Age-related changes in body weight have also been observed during pregnancy. For all three pregnancy ages analyzed (2M, 5M, and 6M–7M), *Atp6v0d2*$^{-/-}$*Mcoln1*$^{-/-}$ mice had significantly lower body weights than their age-matched controls on D0.5 (Fig. 1D–F). However, although this trend was maintained during the rest of the pregnancies for *Atp6v0d2*$^{-/-}$*Mcoln1*$^{-/-}$ mice at pregnancy ages of 5M and 6M to 7M (Fig. 1E and F), the pregnant *Atp6v0d2*$^{-/-}$*Mcoln1*$^{-/-}$ mice at 2M of pregnancy age reached comparable body weights to the age-matched controls toward the late stage of pregnancy (Fig. 1D), reflecting increased percentages of body weight gain in the *Atp6v0d2*$^{-/-}$*Mcoln1*$^{-/-}$ mice compared with the control (Fig. 1D).

A similar mating study in *Mcoln1*$^{-/-}$ mice from 2M showed that *Mcoln1*$^{-/-}$ female mice quickly became infertile by 5M (0/7)[11]. *Atp6v0d2*$^{-/-}$*Mcoln1*$^{-/-}$ mice had pregnancy rates of 27.8% (5/18) at 5M and 23.1% (3/13) at 6M to

7M, indicating a partial rescue of fertility at 5M to 7M in *Atp6v0d2*$^{-/-}$*Mcoln1*$^{-/-}$ mice compared with *Mcoln1*$^{-/-}$ mice. However, because of the small sample size and low rescue rate (approximately 25%), no significant difference was observed between the two groups. We did not examine the fertility of virgin *Mcoln1*$^{-/-}$ and *Atp6v0d2*$^{-/-}$*Mcoln1*$^{-/-}$ mice at ≥5M.

General health of Atp6v0d2$^{-/-}$*Mcoln1*$^{-/-}$ *females*

We did not observe any evident abnormal activity, including mating activity, in *Atp6v0d2*$^{-/-}$*Mcoln1*$^{-/-}$ female mice, except for low body weight before 5M (Fig. 1D–F). Rigid hind legs began to appear in a few mice at ~6M, similar to those reported for *Mcoln1*$^{-/-}$ mice[23]. Of the 13 *Atp6v0d2*$^{-/-}$*Mcoln1*$^{-/-}$ females remaining in the 6M to 7M fertility test group (Fig. 1B and C), all three pregnant mice were euthanized because of dystocia at 8M. Among the remaining 10 *Atp6v0d2*$^{-/-}$*Mcoln1*$^{-/-}$ females at the end of the fertility test (8M), five had paralyzed hind legs, and the other five could still move around; all of them were skinny with little fat tissue and had an enlarged bladder filled with urine. The hyperdistended/hypertrophic bladder phenotype was also reported in *Mcoln1*$^{-/-}$ mice[23,30].

Three of 11 of Atp6v0d2$^{-/-}$*Mcoln1*$^{-/-}$ *females had normal P4 levels compared with 0 of 18 of Mcoln1*$^{-/-}$ *females at 5M–6M*

When the *Atp6v0d2*$^{-/-}$*Mcoln1*$^{-/-}$ mice were 5M, we randomly selected four control mice and 11 *Atp6v0d2*$^{-/-}$*Mcoln1*$^{-/-}$ mice in the fertility test cohort for serum collection on D3.5. All four control mice had serum P4 levels of >20 ng/mL, whereas some *Atp6v0d2*$^{-/-}$*Mcoln1*$^{-/-}$ mice had considerably lower P4 levels. Based on P4 levels (<12 ng/mL as low P4) and fertility history, 11 *Atp6v0d2*$^{-/-}$*Mcoln1*$^{-/-}$ mice were divided into three subgroups (Fig. 2A). In the low P4 and infertile group (n = 2), two mice had low P4 levels and no pregnancy despite continuous mating activity, as indicated by vaginal plugs. The infertility rate (2/11, 18.2%) was comparable with that of the entire *Atp6v0d2*$^{-/-}$*Mcoln1*$^{-/-}$ cohort (8/40, 20%). In the low P4 and once fertile group (n = 6), six mice had low P4 levels and had previously produced one to two litters during fertility testing. In the normal P4 group (n = 3), three mice had comparable P4 levels with that of the controls and had previously produced one to two litters during the fertility test. The percentage of *Atp6v0d2*$^{-/-}$*Mcoln1*$^{-/-}$ mice with normal P4 levels (3/11, 27.3%) at 5M (Fig. 2A) was consistent with the pregnancy rate at 5M in the cohort (5/18 = 27.8%) (Fig. 1B). The serum E_2 levels in control and *Atp6v0d2*$^{-/-}$*Mcoln1*$^{-/-}$ mice at 5M were comparable (Fig. 2B). Since P4 levels reach a plateau by D3.5 in mice[7], comparable P4 levels are expected between D3.5 and D4.5 of early pregnancy in the same mice. We have previously reported that 100% (18/18) of 5M to 6M *Mcoln1*$^{-/-}$ mice had P4 deficiency at D4.5 (n = 7) in the first study[11] and at D3.5 (n = 6) and D4.5 (n = 5) in the second study[12]. Normal P4 levels were observed in 0% (0/18) of *Mcoln1*$^{-/-}$ mice and 27.3% (3/11, P = 0.0452; two-tailed Fisher's exact test) of *Atp6v0d2*$^{-/-}$*Mcoln1*$^{-/-}$ mice, indicating a partial rescue effect on P4 levels upon the additional deletion of *Atp6v0d2* in *Mcoln1*$^{-/-}$ mice during early pregnancy.

Comparable follicle morphology and CL counts in the ovaries of control, Mcoln1$^{-/-}$*, and Atp6v0d2*$^{-/-}$*Mcoln1*$^{-/-}$ *mice at 5M*

During early pregnancy, P4 is primarily synthesized in the CL, which normally develops from ovulated follicles. We examined follicles and CLs in the D3.5 ovaries from 5M control, *Mcoln1*$^{-/-}$, and *Atp6v0d2*$^{-/-}$*Mcoln1*$^{-/-}$ mice. No morphological differences in the follicles at different stages and no significant differences in the CL counts were observed among the three groups (data not shown).

Completely or partially restored Atp6v0d2$^{-/-}$*Mcoln1*$^{-/-}$ *CL morphology compared with Mcoln1*$^{-/-}$ *CL at 5M*

Representative histological images of D3.5 ovaries are shown in Fig. 3A–H1. In the control CLs, there were defined corpus luteal cords, which are clusters of luteal cells surrounded by endothelial cells, and the luteal cells generally appeared round with a large cytoplasm (Fig. 3A–A1). Regressing CLs from the previous cycle had large empty spaces and some dense nuclei, but no amorphous cellular debris (Fig. 3F and F1). In the *Mcoln1*$^{-/-}$ CLs (Fig. 3B and B1), corpus luteal cord and vasculature were less defined compared with the control CLs (Fig. 3A and A1); luteal cells had foamy cytoplasm, an indication of vacuolization; all CLs in the 6 *Mcoln1*$^{-/-}$ ovaries (1 ovary/mouse) examined

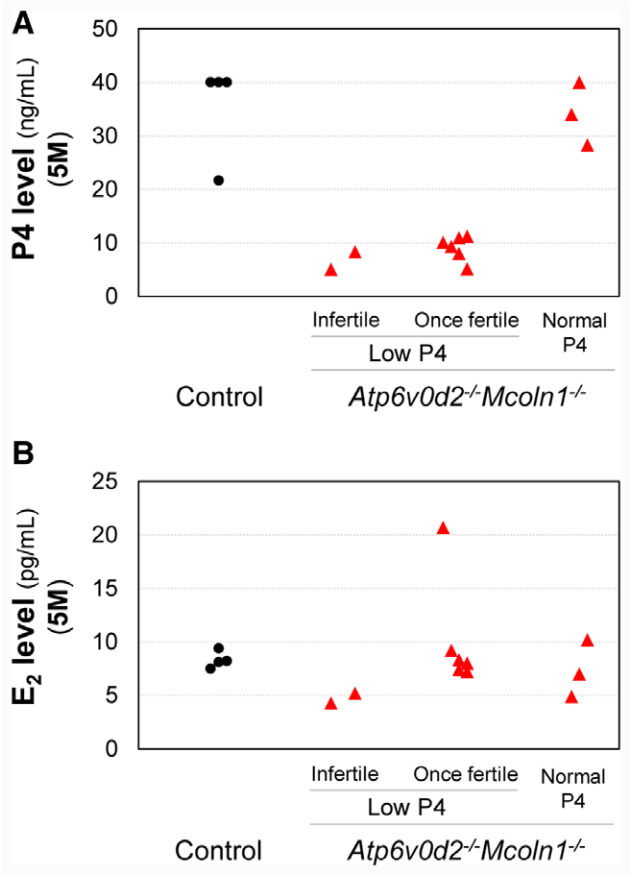

Fig. 2. Serum P4 level (A) and estrogen (E_2) level (B). A subset of mice at 5M was randomly selected from the cohort in the fertility test. Serum was collected at post-coitum day 3.5 (D3.5). n = 4 for control mice, black dots; and n = 11 for *Atp6v0d2*$^{-/-}$*Mcoln1*$^{-/-}$ mice, red triangles. *Atp6v0d2*$^{-/-}$*Mcoln1*$^{-/-}$ mice were divided into three subgroups as follows: low P4 and infertile (n = 2), low P4 and once fertile (n = 6), and normal P4 (n = 3). P4: progesterone.

were in two main categories: the majority CLs with medium to extensive amorphous cell debris, an indication of cell death due to cellular degeneration (Fig. 3B and B1), and a few regressing CLs without evident amorphous cellular debris but large empty spaces and some dense nuclei (0–2 CLs/ovary) (Fig. 3G and G1), similar as seen in the control (Fig. 3F1). All six *Mcoln1*$^{-/-}$ ovaries examined had at least one CL with extensive amorphous cellular debris (Fig. 3I).

We sectioned two ovaries (1 ovary/mouse) from each of the three *Atp6v0d2*$^{-/-}$*Mcoln1*$^{-/-}$ subgroups. In the two ovaries from the only two *Atp6v0d2*$^{-/-}$*Mcoln1*$^{-/-}$ mice with low P4 and infertility, one had a CL with amorphous cellular debris and undefined luteal cords (Fig. 3C and C1) and the other ovary had two CLs, one of which had undifferentiated luteal cells but no evident amorphous cell debris (Fig. 3H and H1) and the other had similar morphology as shown in Fig. 3F1 and G1, most likely a regressing CL from a previous cycle. In the two *Atp6v0d2*$^{-/-}$*Mcoln1*$^{-/-}$ ovaries from the low P4 and once fertile subgroup, the CLs rarely had amorphous cellular debris as seen in Fig. 3B1 and C1 or empty spaces and dense nuclei as seen in Fig. 3F1 and G1, but most luteal cells did not have a large cytoplasmic area (Fig. 3D and D1) compared with those in Fig. 3A1 and E1, indicating restored cell survival but not luteal cell differentiation. In the two *Atp6v0d2*$^{-/-}$*Mcoln1*$^{-/-}$ ovaries from the normal P4 subgroup, the CLs had a similar morphology (Fig. 3E and E1) as the control CLs (Fig. 3A and A1), with restored cell survival and luteal cell differentiation. These data demonstrate a general recovery of CL morphology to different degrees in *Atp6v0d2*$^{-/-}$*Mcoln1*$^{-/-}$ CLs (Fig. 3C–E1, H–H1) compared with *Mcoln1*$^{-/-}$ CLs (Fig. 3B and B1). Ovarian histology revealed restored cell survival, as indicated by reduced amorphous cellular debris in *Atp6v0d2*$^{-/-}$*Mcoln1*$^{-/-}$ CLs (1/6 *vs.* 6/6 *Mcoln1*$^{-/-}$ ovaries with significant amorphous cell debris in the CLs) (Fig. 3I). However, restoration of luteal cell differentiation, indicated by round luteal cells with a large cytoplasm, only occurred in *Atp6v0d2*$^{-/-}$*Mcoln1*$^{-/-}$ mice with normal P4 levels (Fig. 4E–4E1).

Varied Col IV expression patterns in Atp6v0d2$^{-/-}$*Mcoln1*$^{-/-}$ *CL at 5M*

Col IV is a marker of the basal lamina of endothelial cells. It is highly expressed in the CL but not in the follicles[11,26], corresponding to high vasculature in the CL but not in the follicles[31]. Immunofluorescence of Col IV in the control ovary revealed a continuous net-like Col IV expression pattern surrounding spaces without Col IV staining, reflecting endothelial cells wrapping around clusters of luteal cells in the luteal cord (Fig. 3J–3J1). In the age-matched D3.5 *Mcoln1*$^{-/-}$ CLs, the overall Col IV intensity under low magnification (Fig. 3K) was not less than that in the control (Fig. 3J), but the spaces wrapped around by the net-like Col IV expression were smaller (Fig. 3K1) than those in the control (Fig. 3J1), an indication of under-differentiated luteal cells/ under-developed luteal cords in *Mcoln1*$^{-/-}$ CL. Similar Col IV staining patterns in *Mcoln1*$^{-/-}$ CLs (Fig. 3K and K1) were also observed in *Atp6v0d2*$^{-/-}$*Mcoln1*$^{-/-}$ CLs with low P4 levels, regardless of fertility history (Fig. 3L, L1, and M). Among the three CLs shown in Fig. 3M, two CLs had similar Col IV expression patterns as seen in Fig. 3K1 and L1; one CL had considerably lower overall Col IV intensity (Fig. 3M) than the other two CLs, and Col IV staining was discontinuous (Fig. 3M1), which was most likely a regressing CL from a previous cycle. The CLs from *Atp6v0d2*$^{-/-}$*Mcoln1*$^{-/-}$ mice with normal P4 levels had comparable Col IV expression levels and expression patterns (Fig. 3N–N1) to control CLs (Fig. 3J–J1). Col IV staining revealed no lack of neovascularization in *Mcoln1*$^{-/-}$ and *Atp6v0d2*$^{-/-}$*Mcoln1*$^{-/-}$ CLs.

Lipid accumulation associated with P4 deficiency in Atp6v0d2$^{-/-}$*Mcoln1*$^{-/-}$ *CLs at 5M*

Lysosomal storage disorder MLIV caused by mutations in *MCOLN1* gene is associated with lipid accumulation[25,32]. Lipid droplets contain cholesterol, the precursor for P4 synthesis[33]. Nile Red was used to detect lipid droplets in the CL[11,12,26]. The lipid droplets in the control CLs were relatively small and uniform in the control CLs, some were too small to be distinctive in the image (Fig. 4A and A1). Those in the *Mcoln1*$^{-/-}$ CLs had varied sizes with increased number of larger ones (Fig. 4B and B1). The lipid droplets in *Atp6v0d2*$^{-/-}$*Mcoln1*$^{-/-}$ CLs with low P4 levels also had larger sizes (Fig. 4C and D1) similar as that in the *Mcoln1*$^{-/-}$ CLs (Fig. 4B and B1). The lipid droplets in the *Atp6v0d2*$^{-/-}$*Mcoln1*$^{-/-}$ CLs with normal P4 levels (Fig. 4E–4E1) were relatively fine and uniform as those in the control (Fig. 4A and A1). These data indicate restored lipid droplet sizes in the CLs of *Atp6v0d2*$^{-/-}$*Mcoln1*$^{-/-}$ mice with normal P4 (Fig. 4E1) but no obvious recovery in the CLs of *Atp6v0d2*$^{-/-}$*Mcoln1*$^{-/-}$ mice with P4 deficiency (Fig. 4C1 and D1) compared with those in *Mcoln1*$^{-/-}$ CLs (Fig. 4B1), which had P4 deficiency[11,12].

Recovery of mitochondrial density and StAR expression in CLs of Atp6v0d2$^{-/-}$*Mcoln1*$^{-/-}$ *mice with normal P4 levels at 5M*

P4 synthesis is initiated in the mitochondria, and the rate-limiting step is the transport of cholesterol from the outer to the inner mitochondrial membrane *via* StAR[33,34]. HSP60 is a mitochondrial marker. Both HSP60 and StAR were highly expressed in the cytoplasm of luteal cells in control CLs (Fig. 4F, F1, K, and K1) and CLs from *Atp6v0d2*$^{-/-}$*Mcoln1*$^{-/-}$ mice with normal P4 levels (Fig. 4J, J1, O, and O1). The expression levels in the other three groups with low P4 levels were consistently low (Fig. 4G–I1 and 4L–N1). These results demonstrate the correlation between mitochondrial density, StAR expression, and serum P4 levels, regardless of genotype. The parameters investigated at 5M are summarized in Table 1.

Discussion

One limitation of this study was the lack of direct evidence of the co-localization of the V-ATP subunit ATP6v0d2 (encoded by *Atp6v0d2*) and TRPML1 (encoded by *Mcoln1*) in wild-type luteal cells and their absence in *Atp6v0d2*$^{-/-}$*Mcoln1*$^{-/-}$ luteal cells. We were fortunate to receive a vial of customized anti-TRMPL1 antibody from Dr. Abigail A Soyombo[21] before she closed her lab. Using this antibody, we detected TRPML1 in the ovary, including the luteal cells in the CL[11]. Before the initiation of *Atp6v0d2*$^{-/-}$*Mcoln1*$^{-/-}$ double-knockout mice, we tested a few commercially available anti-ATP6v0d2 and anti-TRPML1 antibodies by immunohistochemistry and immunofluorescence, but none worked. Subsequently, we made customized antibodies while the breeding for generating *Atp6v0d2*$^{-/-}$*Mcoln1*$^{-/-}$ mice was ongoing, but again, none of them worked. We resorted to the literature for support that ATP6v0d2 and TRPML1 are expected to co-localize in some intracellular organelles, especially lysosomes[4], in certain cell types where both ATP6v0d2 and TRPML1 are expressed.

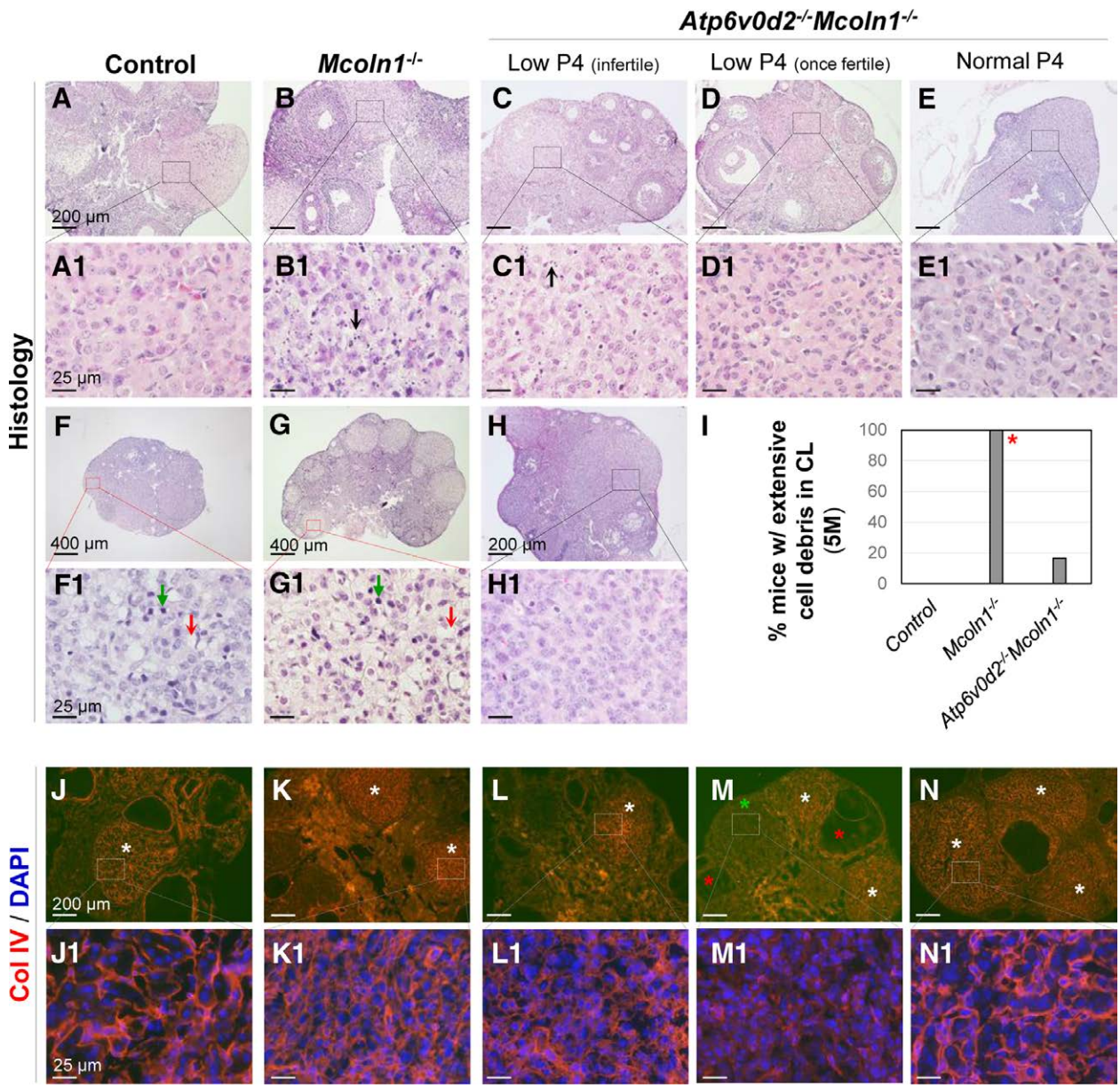

Fig. 3. Histology of CL and Col IV immunofluorescence in the ovaries. Ovaries were from D3.5 5M mice that were in the fertility cohort (control and *Atp6v0d2*$^{-/-}$*Mcoln1*$^{-/-}$) or not in the fertility cohort but were non-virgin (*Mcoln1*$^{-/-}$). Five groups of mice were included: control mice, *Mcoln1*$^{-/-}$ mice, and three subgroups of *Atp6v0d2*$^{-/-}$*Mcoln1*$^{-/-}$ mice (low P4 and infertile, low P4 and once fertile, and normal P4). (A–H1) Hematoxylin and eosin staining in fixed ovaries. Black arrow in (B1) and (C1), amorphous cellular debris; (F1) and (G1), regressing CL from a previous cycle; red arrow in (F1) and (G1), empty cytoplasm; green arrow in (F1) and (G1), dense nucleus. (I) Percentage of mice with extensive amorphous cell debris in the CL of the control, *Mcoln1*$^{-/-}$, and *Atp6v0d2*$^{-/-}$*Mcoln1*$^{-/-}$ groups. n = 4–6/group; * P <0.05, compared with both the control and *Atp6v0d2*$^{-/-}$*Mcoln1*$^{-/-}$ groups. (J–N1) Col IV staining in frozen ovaries. (A, F, J) Control; (B, G, K) *Mcoln1*$^{-/-}$; (C, H, L) *Atp6v0d2*$^{-/-}$*Mcoln1*$^{-/-}$ low P4 and infertile; (D, M) *Atp6v0d2*$^{-/-}$*Mcoln1*$^{-/-}$ low P4 and once fertile; (E, N) *Atp6v0d2*$^{-/-}$*Mcoln1*$^{-/-}$ normal P4. (A1–H1) and (J1–N1) enlarged from the boxed area in (A–H) and (J–N), respectively. Scale bar: 400 μm in (F) and (G); 200 μm in (A–E), (H), (J–N); and 25 μm in (A1–H1) and (J1–N1); *CL; green * in M, most likely a regressing CL from a previous cycle, with lower Col IV staining than other CLs in the section but higher than that in follicles (red * in M). No specific staining in the follicle or CL but autofluorescence in the interstitial areas of the negative control ovaries (data not shown). CL: corpus luteum; Col IV: collagen IV; DAPI: 4′,6′-diamino-2-phenylindole; P4: progesterone.

The CL is a transient gland. An intriguing question is why there is an age-related premature loss of CL function in the *Mcoln1*$^{-/-}$[11] and *Atp6v0d2*$^{-/-}$*Mcoln1*$^{-/-}$ mice. Aging is associated with cellular senescence, which is linked to lysosomal dysfunction[35]. The CL is derived from an ovulated follicle, and cells in an ovarian follicle undergo an aging process[36], which would subsequently subject the CL to the aging process despite the fact that the CL is a transient gland. Indeed, CL tissues from aging cows have diminished functions, to which cellular senescence is a reasonable contributing factor[37]. Since low pH is essential for lysosomal functions, and V-ATPase and TRMPL1 are critical for maintaining the low pH in the lysosomes, disruption of these channels could disrupt lysosomal functions, leading to premature cellular senescence. Lysosomes also regulate cell death processes, such as necrosis and apoptosis[8]. The extensive amorphous cellular debris in the CLs of 5M *Mcoln1*$^{-/-}$ mice indicates degenerative cell death.

CL formation and regression are controlled by the hypothalamic–pituitary–gonadal (HPG) axis, which includes prolactin (PRL) signaling and many local factors. PRL is

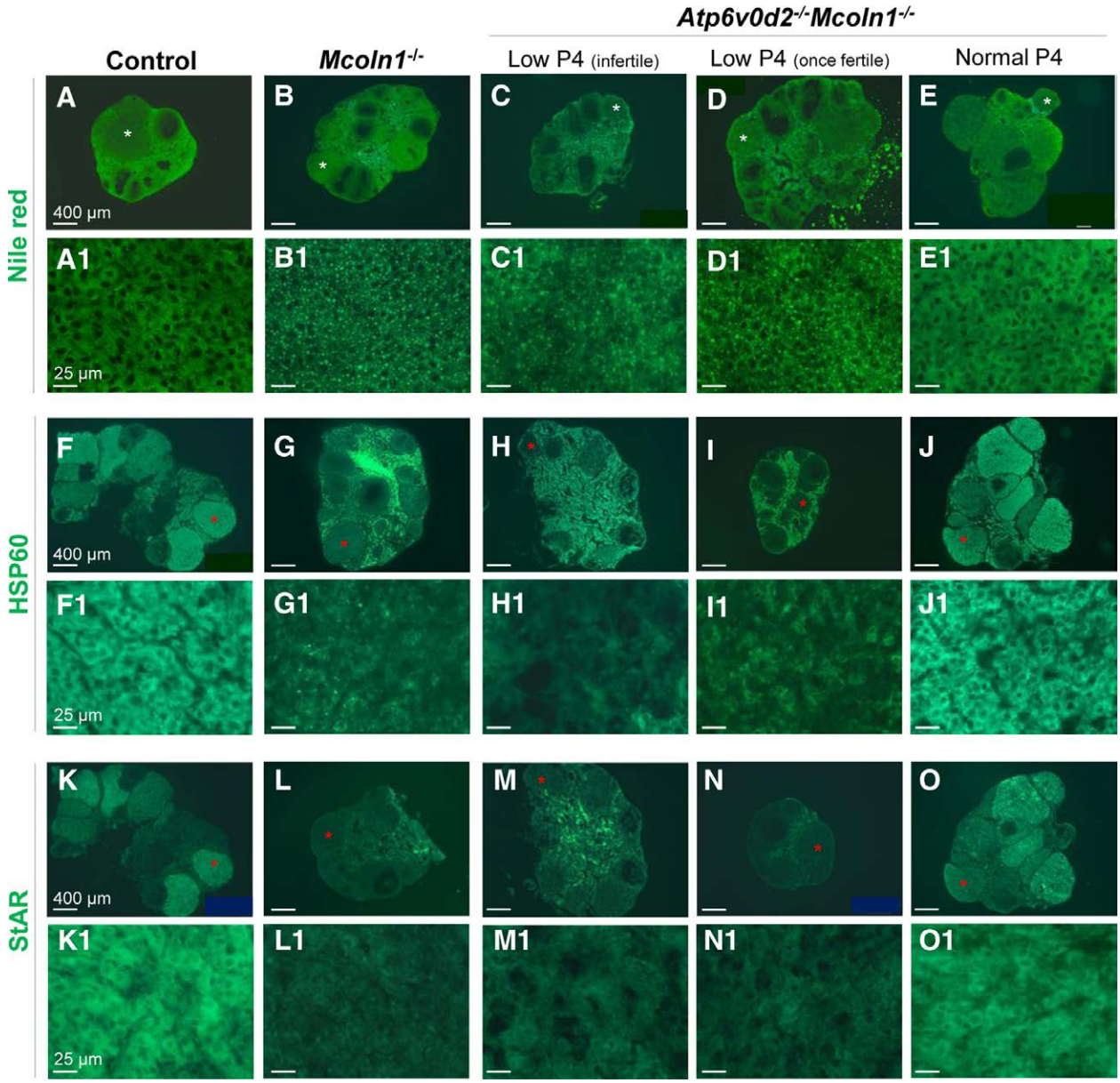

Fig. 4. Nile red staining of lipid droplets and immunofluorescence detection of HSP60 and StAR in frozen ovaries from 5M mice at D3.5. Five groups of mice were included: control mice, *Mcoln1*$^{-/-}$ mice, and three groups of *Atp6v0d2*$^{-/-}$*Mcoln1*$^{-/-}$ mice (low P4 and infertile, low P4 and once fertile, and normal P4). (A–E1) Nile red staining. (F–J1) HSP60. (K–O1) StAR. (A, F, K) Control; (B, G, L) *Mcoln1*$^{-/-}$; (C, H, M) *Atp6v0d2*$^{-/-}$*Mcoln1*$^{-/-}$ low P4 and infertile; (D, I, N) *Atp6v0d2*$^{-/-}$*Mcoln1*$^{-/-}$ low P4 and once fertile; (E, J, O) *Atp6v0d2*$^{-/-}$*Mcoln1*$^{-/-}$ normal P4 level. (A1–O1) Enlarged from the CL labeled with * in (A–O), respectively. Scale bar, 400 μm in (A–O), and 25 μm in (A1–O1). No specific staining in the follicle or CL but autofluorescence in the interstitial areas of the negative control ovaries (data not shown). CL: corpus luteum; HSP60: heat shock protein 60; P4: progesterone; StAR: steroidogenic acute regulatory protein.

secreted from the pituitary gland and activates the PLR receptor (PRLR) in the ovary. The PRL signaling regulates ovarian follicle maturation and ovulation, as well as CL formation, mainly via promoting neovascularization during luteal development, which was revealed by the underdeveloped vasculature in the *Prlr*$^{-/-}$ CL[38–40]. HPG axis and PRL signaling are not main contributing factors for the phenotypes in the *Mcoln1*$^{-/-}$ mice and *Atp6v0d2*$^{-/-}$*Mcoln1*$^{-/-}$ mice based on the following rationales: TRPML1/*Mcoln1* is highly expressed in the luteal cells[11]; *Mcoln1*$^{-/-}$ mice and *Atp6v0d2*$^{-/-}$*Mcoln1*$^{-/-}$ mice have normal ovarian follicles, as well as comparable serum estrogen levels, mating activities, ovulation, and CL formation to their age-matched control mice, suggesting a functional HPG axis in these mice; and the vasculature in the CL, indicated by the Col IV staining, is well developed in the *Mcoln1*$^{-/-}$ mice and *Atp6v0d2*$^{-/-}$*Mcoln1*$^{-/-}$ mice albeit disorganized in the mice with low P4, suggesting that impairment of PRL-PRLR signaling is not evident in these mouse models and that disorganized Col IV staining is most likely caused by the under-differentiated but degenerative luteal cells.

Our previous study has reported that Col IV, a basal lamina marker of endothelial cells, has comparable overall intensity with the interstitial compartment in the D3.5 *Mcoln1*$^{-/-}$ CLs, whereas the control CLs have overall higher expression levels than the interstitial compartment[11]. In the present study, we did not consistently observe this pattern. This difference might be attributable to the different batches of antibodies used in these two studies and/or the varied intensity of autofluorescence in the intestinal compartment (but not in follicles or CLs) that was consistently detected in the negative controls (data not shown).

Table 1.

Summary of the parameters in different groups of mice at 5M.

	Control	*Mcoln1*$^{-/-}$	*Atp6v0d2*$^{-/-}$*Mcoln1*$^{-/-}$		
Parameters	**Normal P4**	**Low P4 and infertile**	**Low P4 and infertile**	**Low P4 and once fertile**	**Normal P4**
Follicle morphology	Comparable				
CL count	Comparable				
Luteal cell debris	–	+++	–/++	–	–
Luteal cell differentiation	+++	–/+	–/+	–/+	+++
Col IV expression level in CL	Comparable				
Col IV expression pattern in CL	Net-like with large spaces	Net-like with small spaces	Net-like with small spaces	Net-like with small spaces	Net-like with large spaces
Size of largest lipid droplets	+	+++	+++	+++	+
HSP60	+++	–/+	–/+	–/+	+++
StAR	+++	–/+	–/+	–/+	+++

+: Higher levels of cell debris, more luteal cell differentiation, larger lipid droplets, or higher expression of HSP60 and StAR. CL: corpora lutea; HSP60: heat shock protein 60; P4: progesterone; StAR: steroidogenic acute regulatory protein.

Regardless, the Col IV expression patterns in the control and *Mcoln1*$^{-/-}$ CLs and no staining in the follicles were consistent in the two studies. Although we observed a partial recovery in CL morphology, for example, less degenerative cell death indicated by reduced amorphous cellular debris in the CLs from *Atp6v0d2*$^{-/-}$*Mcoln1*$^{-/-}$ mice with P4 deficiency but once fertile, no marked difference was observed in the Col IV staining patterns among *Mcoln1*$^{-/-}$ and two *Atp6v0d2*$^{-/-}$*Mcoln1*$^{-/-}$ subgroups with low P4 levels. The CL morphology indicated that these three groups and subgroups lacked well-differentiated luteal cells. This observation indicates that the pattern of Col IV staining, an indicator of endothelial cells, in the CL correlates with luteal cell differentiation and P4 levels, but not cell survival in the CL.

Luteal cell differentiation and P4 levels are also correlated with lipid droplet accumulation and the expression of HSP60 and StAR in the CL. Lipid droplet accumulation is a hallmark of MLIV, which is due to TRPML1 deficiency caused by *MCOLN1* mutations[25,32]. TRPML1 deficiency can lead to mitochondrial fragmentation, likely because of the inefficient autophagolysosomal recycling of mitochondria[41]. The expression of HSP60, a mitochondrial marker, and StAR, which performs the rate-limiting step in steroidogenesis to transport cholesterol from the outer to the inner mitochondrial membrane, is directly related to mitochondrial quantity and function. Comparable lipid droplet accumulation and reduced expression of HSP60 and StAR in the 5M D3.5 *Mcoln1*$^{-/-}$ group and two *Atp6v0d2*$^{-/-}$*Mcoln1*$^{-/-}$ subgroups with low P4 levels would suggest that the level of restoration in the *Atp6v0d2*$^{-/-}$*Mcoln1*$^{-/-}$ CLs of these two subgroups was sufficient to prevent cell degeneration (indicated by amorphous cellular debris) in most CLs but was insufficient to restore the lysosomal functions in regulating lipid droplets and mitochondria. This makes cell survival the fundamental cellular event to be restored first.

There might be a threshold for restoration of other lysosomal functions. We observed that approximately 25% of *Atp6v0d2*$^{-/-}$*Mcoln1*$^{-/-}$ female mice had normal P4 levels and all examined CL parameters at 5M (Table 1), indicating full recovery of lysosomal function in the CL of this subgroup of *Atp6v0d2*$^{-/-}$*Mcoln1*$^{-/-}$ mice compared with that in the *Mcoln1*$^{-/-}$ CL. Consistently, approximately 25% of *Atp6v0d2*$^{-/-}$*Mcoln1*$^{-/-}$ female mice remained fertile until 7M with term pregnancies continuing until 8M. We did not continue the fertility tests because of progressive neurological defects. The molecular mechanisms leading to the full recovery of CL function and fertility in approximately 25% of *Atp6v0d2*$^{-/-}$*Mcoln1*$^{-/-}$ female mice and partial recovery of CL cell survival only in the remaining approximately 75% of *Atp6v0d2*$^{-/-}$*Mcoln1*$^{-/-}$ female mice at 5M remain to be investigated. One potential explanation for this is that ATP6V0d2 plays various roles in CLs, leading to varied outcomes. TRMPL1 was shown to be a lysosomal channel that can leak out H^+ to coregulate lysosomal pH with V-ATPase[25]. TRMPL1 deficiency in cells from MLIV patients and *Mcoln1*$^{-/-}$ mice leads to overly acidified lysosomes due to accumulation of H^+ in the lysosomal lumen[25]. Therefore, if V-ATPase is impaired in pumping H^+ into the lysosomal lumen, the accumulation of H^+ in the lysosomal lumen would be alleviated in the TRMPL1 deficient lysosomes. When such an alleviation reaches a threshold to restore the lysosomal ionic homeostasis and membrane potential, the lysosomal functions will be restored. In the CLs where ATP6V0d2 plays a significant role in V-ATPase activity for pumping H^+ in the lysosomal lumen and its role could not be compensated by ATP6V0d1 or other channels, ATP6V0d2 deficiency will lead to reduced V-ATPase activity and less H^+ pumped into the lysosomal lumen, reaching a new balance for the lysosome to be fully functional. In the CLs where ATP6V0d2 has a lesser contribution to V-ATPase activity, ATP6V0d2 deficiency will correct the imbalance caused by TRPML1 deficiency to a lesser extent, such as improving cell survival in the CL but no other parameters that we had examined (Table 1 and Fig. 5).

The assumed restoration of lysosomal functions seems to be cell type specific, most likely due to ATP6V0d2 being the more tissue-specific d subunit of the V-ATPase, and cell/tissue-specific functions of V-ATPase subunits are common[14,16]. We observed 60% in 5M group and 100% in 6M to 7M group of pregnant *Atp6v0d2*$^{-/-}$*Mcoln1*$^{-/-}$ mice with dystocia. Since the most common cause of dystocia is inefficient uterine myometrial contraction, the age-dependent progressively increasing rates of dystocia in pregnant *Atp6v0d2*$^{-/-}$*Mcoln1*$^{-/-}$ mice indicate that lysosomal functions in myometrial cells are important for uterine contraction. Studies have connected lysosomal functions with parturition[8], but systemic studies remain lacking. Our initial reason for analyzing lysosomal function in the uterus was the dramatic upregulation of *Atp6v0d2* in the uterine LE and uterine epithelial acidification upon the initiation of embryo implantation[9,10]. We have not examined *Atp6v0d2* expression in the myometrium toward parturition. We previously detected *Atp6v0d2* in uterine LE of D4.5 mouse uterus but *Atp6v0d2* was undetectable in D4.5 myometrium[10]. If ATP6V0d2 remains undetectable in the myometrium throughout the pregnancy, the dystocia in *Atp6v0d2*$^{-/-}$*Mcoln1*$^{-/-}$ mice would be contributed by *Mcoln1* deletion. Using the gift

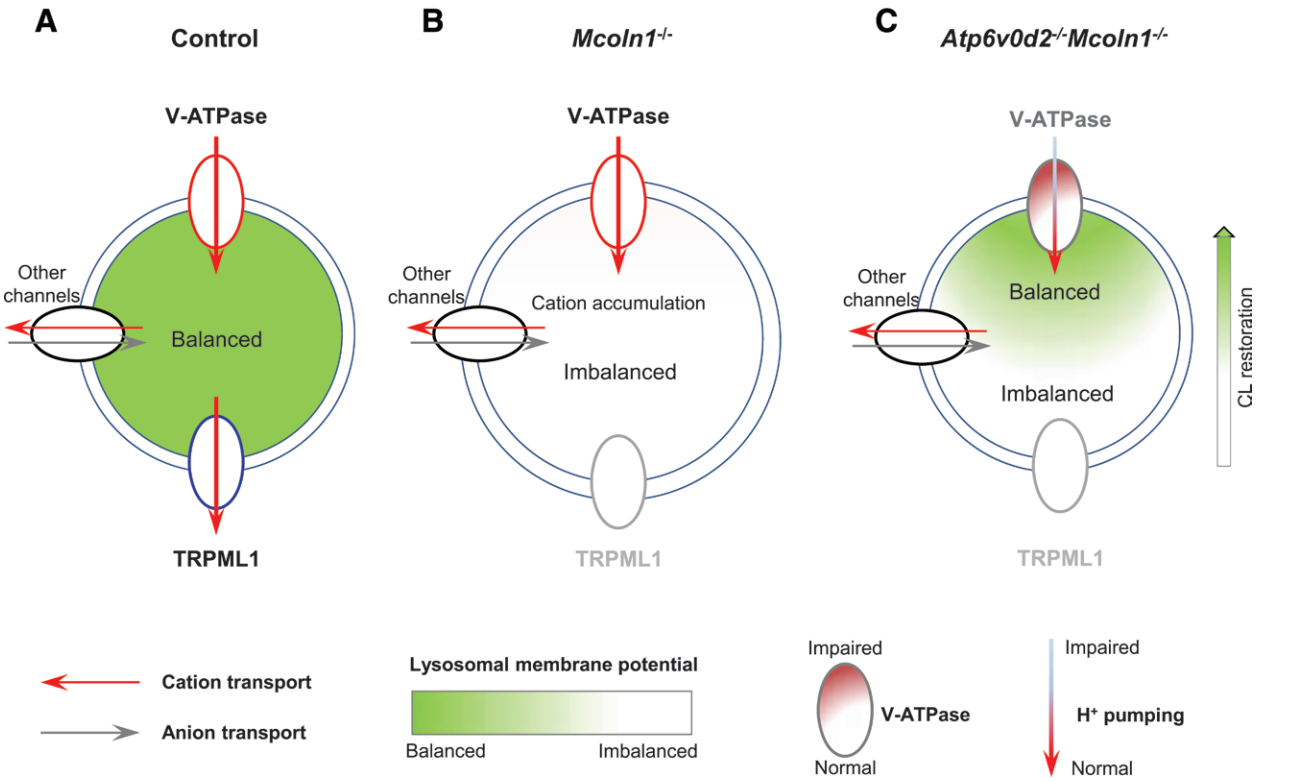

Fig. 5. Proposed model for varied rescuing effects in *Atp6v0d2*$^{-/-}$*Mcoln1*$^{-/-}$ CL compared with *Mcoln1*$^{-/-}$ CL. *Atp6v0d2* encodes one of the two ATP6V0d subunits for V-ATPase, which pumps H^+ from the cytosol to the lysosomal lumen. *Mcoln1* encodes TRPML1, a cation counter ion channel that transports cations, including H^+, from the lysosomal lumen to the cytosol. TRPML1 deficiency leads to MLIV, a progressive and severe lysosomal storage disorder with a slow onset. The proposed model is for D3.5 CLs from 5M mice that have been in mating since 2M. (A) Control. Balanced lysosomal lumen ionic homeostasis, indicated by the green lumen. (B) *Mcoln1*$^{-/-}$. Imbalanced lysosomal ionic components, expected to be caused by accumulation of cations in the lysosomal lumen resulted from TRPML1 deficiency, indicated by the white lumen. (C) *Atp6v0d2*$^{-/-}$*Mcoln1*$^{-/-}$. Gradient rescue of lysosomal lumen ionic homeostasis by additional ATP6V0d2 deficiency. In the CLs where ATP6V0d2 deficiency leads to more impairment of V-ATPase activity in pumping H^+ in the lysosomal lumen, the imbalance caused by TRPML1 deficiency could be canceled out to reach a new balance for the lysosome to be fully functional, indicated by gradient reddish V-ATPase (more impairment), grayish arrow (less H^+ pumping), and greenish lysosomal lumen (functional lysosome). In the CLs where ATP6V0d2 deficiency has no or minor impairment of V-ATPase activity, the imbalance caused by TRPML1 deficiency could not or could only be partially corrected, indicated by gradient whitish V-ATPase, reddish arrow, and white lysosomal lumen. CL: corpus luteum; MLIV: mucolipidosis type IV; TRPML1: transient receptor potential cation channel, mucolipin subfamily, member 1.

anti-TRPML1 antibody from Dr. Soyombo[21], we detected TRPML1 in the mouse myometrium during early pregnancy (unpublished observation). We have not examined TRPML1 expression in the mouse myometrium toward parturition. These observations suggest a novel function of TRPML1 in parturition. The function of TRMPL1 in smooth muscle contractility is also shown in the bladder[23,30].

This study demonstrated that deletion of both *Atp6v0d2* and *Mcoln1* in female mice could restore CL cell survival in most mice and restore fertility in a ~25% of *Atp6v0d2*$^{-/-}$*Mcoln1*$^{-/-}$ mice at 5M to 7M compared with the deletion of *Mcoln1* alone. Although the mechanisms underlying the various effects remain to be investigated, this study provides *in vivo* genetic evidence for the coordination between different lysosomal channels in CL function.

Acknowledgments

The authors thank the Office of the Vice President for Research, Interdisciplinary Toxicology Program, and the Department of Physiology and Pharmacology at the University of Georgia, and the National Institutes of Health (NIH) for their financial support. Serum P4 and E_2 levels were determined at the University of Virginia Center for Research in Reproduction Ligand Assay and Analysis Core, which was supported by the Eunice Kennedy Shriver NICHD/NIH (NCTRI) Grant P50-HD28934.

Author contributions

Y.L. and X.Y. conceived the project and designed the experiments; A.E.E.Z. generated the *Atp6v0d2*$^{-/-}$*Mcoln1*$^{-/-}$ mice; A.E.E.Z., Y.L., Z.W., S.V., and J.B. maintained the mouse colony; A.E.E.Z. collected some preliminary data; Y.L. performed majority of the experiments and data analyses; J.M.H. conducted immunofluorescence work; Z.W., T.E.M., and Y.W. assisted in the experiments; J.M.H., T.E.M., T.Z., C.L.A., V.A.A., K.R.K., H.N.G., S.X., and X.Y. assisted in the data analyses; Y.L. and X.Y. wrote the manuscript; J.M.H., T.E.M., Z.W., and S.X. assisted in the manuscript revision; all the authors reviewed the manuscript; X.Y. supervised the entire project.

Funding(s)

This study was funded by NIH R01HD065939 (co-funded by ORWH and NICHD), NIH R03HD097384, and NIH R03 HD100652 to X.Y.

Conflicts of interest

All authors declare no conflicts of interest. Xiaoqin Ye is Editorial Board member of *Reproductive and Developmental Medicine*. The article was subject to the journal's standard procedures, with peer review handled independently of these Editorial Board member and their research groups.

Data availability statement

Data are available upon request.

References

[1] Mindell JA. Lysosomal acidification mechanisms. Annu Rev Physiol 2012;74:69–86. doi:10.1146/annurev-physiol-012110-142317.

[2] Hu M, Zhou N, Cai W, *et al*. Lysosomal solute and water transport. J Cell Biol 2022;221(11):e202109133. doi:10.1083/jcb.202109133.

[3] DiCiccio JE, Steinberg BE. Lysosomal pH and analysis of the counter ion pathways that support acidification. J Gen Physiol 2011;137(4):385–390. doi:10.1085/jgp.201110596.

[4] Xu H, Ren D. Lysosomal physiology. Annu Rev Physiol 2015;77:57–80. doi:10.1146/annurev-physiol-021014-071649.

[5] Li P, Gu M, Xu H. Lysosomal ion channels as decoders of cellular signals. Trends Biochem Sci 2019;44(2):110–124. doi:10.1016/j.tibs.2018.10.006.

[6] Ye X, Hama K, Contos JJ, *et al*. LPA3-mediated lysophosphatidic acid signalling in embryo implantation and spacing. Nature 2005;435(7038):104–108. doi:10.1038/nature03505.

[7] Ye X. Uterine luminal epithelium as the transient gateway for embryo implantation. Trends Endocrinol Metab 2020;31(2):165–180. doi:10.1016/j.tem.2019.11.008.

[8] Li Y, Wang Z, Andersen CL, *et al*. Functions of lysosomes in mammalian female reproductive system. Reprod Dev Med 2020;4(2):109–122. doi:10.4103/2096-2924.288025.

[9] Xiao S, Diao H, Zhao F, *et al*. Differential gene expression profiling of mouse uterine luminal epithelium during periimplantation. Reprod Sci 2014;21(3):351–362. doi:10.1177/1933719113497287.

[10] Xiao S, Li R, El Zowalaty AE, *et al*. Acidification of uterine epithelium during embryo implantation in mice. Biol Reprod 2017;96(1):232–243. doi:10.1095/biolreprod.116.144451.

[11] Wang Z, El Zowalaty AE, Li Y, *et al*. Association of luteal cell degeneration and progesterone deficiency with lysosomal storage disorder mucolipidosis type IV in *Mcoln1*$^{-/-}$ mouse model. Biol Reprod 2019;101(4):782–790. doi:10.1093/biolre/ioz126.

[12] Wang Z, Li Y, Andersen CL, *et al*. Exogenous estrogen partially rescues progesterone deficiency and autophagosome enlargement in Mcoln1–/– mouse model with lysosomal storage disorder. Reprod Dev Med 2024;8(4):197–205. doi:10.1097/RD9.0000000000000109.

[13] Diao H, Xiao S, Zhou T, *et al*. Attenuated retinoic acid signaling is among the early responses in mouse uterus approaching embryo attachment. Reprod Dev Med 2024;8(1):61–65. doi:10.1097/RD9.0000000000000090.

[14] Lee SH, Rho J, Jeong D, *et al*. v-ATPase V0 subunit d2-deficient mice exhibit impaired osteoclast fusion and increased bone formation. Nat Med 2006;12(12):1403–1409. doi:10.1038/nm1514.

[15] Eaton AF, Merkulova M, Brown D. The H$^+$-ATPase (V-ATPase): from proton pump to signaling complex in health and disease. Am J Physiol Cell Physiol 2021;320(3):C392–C414. doi:10.1152/ajpcell.00442.2020.

[16] Toei M, Saum R, Forgac M. Regulation and isoform function of the V-ATPases. Biochemistry 2010;49(23):4715–4723. doi:10.1021/bi100397s.

[17] Wang S, Han Y, Nabben M, *et al*. Endosomal v-ATPase as a sensor determining myocardial substrate preference. Metabolites 2022;12(7):579. doi:10.3390/metabo12070579.

[18] Forgac M. Structure and properties of the vacuolar H$^+$-ATPases. J Biol Chem 1999;274(19):12951–12954. doi:10.1074/jbc.274.19.12951.

[19] Li P, Hu M, Wang C, *et al*. LRRC8 family proteins within lysosomes regulate cellular osmoregulation and enhance cell survival to multiple physiological stresses. Proc Natl Acad Sci U S A 2020;117(46):29155–29165. doi:10.1073/pnas.2016539117.

[20] Venkatachalam K, Wong CO, Zhu MX. The role of TRPMLs in endolysosomal trafficking and function. Cell Calcium 2015;58(1):48–56. doi:10.1016/j.ceca.2014.10.008.

[21] Chandra M, Zhou H, Li Q, *et al*. A role for the Ca2$^+$ channel TRPML1 in gastric acid secretion, based on analysis of knockout mice. Gastroenterology 2011;140(3):857–867. doi:10.1053/j.gastro.2010.11.040.

[22] Wang W, Zhang X, Gao Q, *et al*. TRPML1: an ion channel in the lysosome. Handb Exp Pharmacol 2014;222:631–645. doi:10.1007/978-3-642-54215-2_24.

[23] Venugopal B, Browning MF, Curcio-Morelli C, *et al*. Neurologic, gastric, and opthalmologic pathologies in a murine model of mucolipidosis type IV. Am J Hum Genet 2007;81(5):1070–1083. doi:10.1086/521954.

[24] Di Paola S, Scotto-Rosato A, Medina DL. TRPML1: The Ca^{2+} retaker of the lysosome. Cell Calcium 2018;69:112–121. doi:10.1016/j.ceca.2017.06.006.

[25] Soyombo AA, Tjon-Kon-Sang S, Rbaibi Y, *et al*. TRP-ML1 regulates lysosomal pH and acidic lysosomal lipid hydrolytic activity. J Biol Chem 2006;281(11):7294–7301. doi:10.1074/jbc.M508211200.

[26] El Zowalaty AE, Li R, Zheng Y, *et al*. Deletion of RhoA in progesterone receptor-expressing cells leads to luteal insufficiency and infertility in female mice. Endocrinology 2017;158(7):2168–2178. doi:10.1210/en.2016-1796.

[27] Li R, Zhao F, Diao H, *et al*. Postweaning dietary genistein exposure advances puberty without significantly affecting early pregnancy in C57BL/6J female mice. Reprod Toxicol 2014;44:85–92. doi:10.1016/j.reprotox.2013.12.003.

[28] Zhao F, Zhou J, El Zowalaty AE, *et al*. Timing and recovery of postweaning exposure to diethylstilbestrol on early pregnancy in CD-1 mice. Reprod Toxicol 2014;49(C):48–54. doi:10.1016/j.reprotox.2014.07.072.

[29] Wang Y, Liu M, Johnson SB, *et al*. Doxorubicin obliterates mouse ovarian reserve through both primordial follicle atresia and overactivation. Toxicol Appl Pharmacol 2019;381:114714. doi:10.1016/j.taap.2019.114714.

[30] Griffin CS, Alvarado MG, Yamasaki E, *et al*. The intracellular Ca^{2+} release channel TRPML1 regulates lower urinary tract smooth muscle contractility. Proc Natl Acad Sci U S A 2020;117(48):30775–30786. doi:10.1073/pnas.2016959117.

[31] Duffy DM, Ko C, Jo M, *et al*. Ovulation: parallels with inflammatory processes. Endocr Rev 2019;40(2):369–416. doi:10.1210/er.2018-00075.

[32] Wakabayashi K, Gustafson AM, Sidransky E, *et al*. Mucolipidosis type IV: an update. Mol Genet Metab 2011;104(3):206–213. doi:10.1016/j.ymgme.2011.06.006.

[33] Christenson LK, Devoto L. Cholesterol transport and steroidogenesis by the corpus luteum. Reprod Biol Endocrinol 2003;1:90. doi:10.1186/1477-7827-1-90.

[34] Manna PR, Dyson MT, Stocco DM. Regulation of the steroidogenic acute regulatory protein gene expression: present and future perspectives. Mol Hum Reprod 2009;15(6):321–333. doi:10.1093/molehr/gap025.

[35] Tan JX, Finkel T. Lysosomes in senescence and aging. EMBO Rep 2023;24(11):e57265. doi:10.15252/embr.202357265.

[36] Zhao H, Wang Y, Yang Y. Follicular development and ovary aging: single-cell studies. Biol Reprod 2023;109(4):390–407. doi:10.1093/biolre/ioad080.

[37] Hori K, Matsuyama S, Nakamura S, *et al*. Age-related changes in the bovine corpus luteum function and progesterone secretion. Reprod Domest Anim 2019;54(1):23–30. doi:10.1111/rda.13303.

[38] Bachelot A, Binart N. Reproductive role of prolactin. Reproduction 2007;133(2):361–369. doi:10.1530/REP-06-0299.

[39] Grosdemouge I, Bachelot A, Lucas A, *et al*. Effects of deletion of the prolactin receptor on ovarian gene expression. Reprod Biol Endocrinol 2003;1:12. doi:10.1186/1477-7827-1-12.

[40] Le JA, Wilson HM, Shehu A, *et al*. Generation of mice expressing only the long form of the prolactin receptor reveals that both isoforms of the receptor are required for normal ovarian function. Biol Reprod 2012;86(3):86. doi:10.1095/biolreprod.111.095927.

[41] Jennings JJ Jr, Zhu JH, Rbaibi Y, *et al*. Mitochondrial aberrations in mucolipidosis Type IV. J Biol Chem 2006;281(51):39041–39050. doi:10.1074/jbc.M607982200.

Edited by: Yong-Qing Zhu

How to cite this article: Li Y, El Zowalaty AE, Hancock JM, Wang Z, Martin TE, Zhan T, Wang Y, Andersen CL, Viswanathan S, Bromfield J, Atluri VA, Kallish KR, Grismer HN, Xiao S, Ye X. *Atp6v0d2* deficiency partially restores defects in *Mcoln1*-deficient mouse corpus luteum. Reprod Dev Med 2025;9(1):11–21. doi: 10.1097/RD9.0000000000000116